International Refereed Journal of Engineering and Science (IRJES)
ISSN (Online) 2319-183X, (Print) 2319-1821
Volume 1, Issue 3(November 2012), PP.13-22
www.irjes.com

Research on a method for distinguishing small retinal haemorrhages from dust artefacts using HLS colour space

N. Suzuki
(Department of Clinical Engineering, Hiroshima International University Univ., Japan)

ABSTRACT : *We aimed to distinguish small retinal haemorrhages, observed in early diabetic retinopathy, from dust artefacts on fundus cameras. For this purpose, we built an experimental device with the same optical system as that of a fundus camera. This experimental device photographed artificial eyes. The fundus was a hemispherical cup made of polythene terephthalate and painted with a matte colour. Fundus images of five patients with diabetic retinopathy were obtained. Paint Shop Pro was used to measure the red-green-blue (RGB) colour space of four areas: the haemorrhagic area, the perihaemorrhagic area, the dust artefact and the periartefact area. RGB values were transformed from these images to the HLS (hue, lightness, and saturation) colour space. In the HLS colour space, lightness and saturation enabled distinction of haemorrhages from dust artefacts under almost all conditions; however, hue enabled this distinction under certain conditions only.*
Keywords - *Diabetic retinopathy, small retinal haemorrhage, HLS Colour space, and dust artifact*

I. INTRODUCTION

According to a study conducted in 1999 in the US, the number of American patients with diabetes was estimated to increase from 16 million to 30 million over the next 30 years [1]. In comparison, the number of Japanese diabetes patients, including potential patients, was 16.2 million in 2005 [2]. Many patients with diabetic retinopathy require regular ophthalmological examinations to prevent loss of eyesight [3]–[6]. Early diagnosis is very important; however, many haemorrhages are minuscule [7]–[9], and detection of small retinal haemorrhages in patients with cloudy ocular media, such as a cataract, is difficult. Moreover, as shown in Fig. 1, magnified images taken with a fundus camera can be unclear. The introduction of the paper should explain the nature of the problem, previous work, purpose, and the contribution of the paper. The contents of each section may be provided to understand easily about the paper.

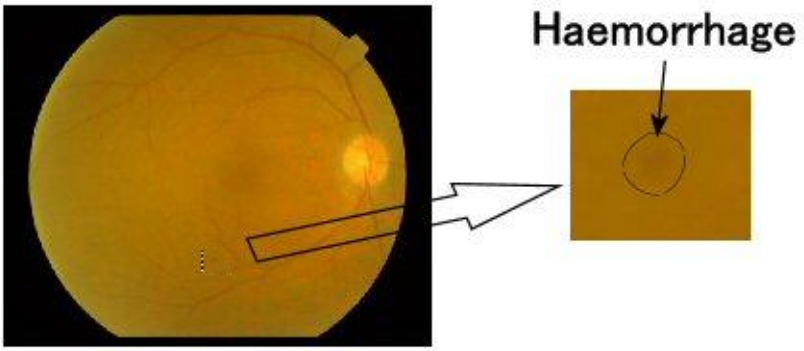

Fig.1 The area of small retinal haemorrhage in the fundus image of patient with diabetic retinopathy

A picture taken of several house dust particles flying around in a room would have a number of white spots on it [10], [11]. These spots are reflections from the room dust particles caused by the camera's flash. Many of the room dust particles are out of focus and the flash reflected from them is stronger than the light reflected from a more distant object. These white spots are called dust artefacts [12]–[14]. If the camera's object lens is dusty, the reflected light from the objects will be obscured by dust particles and black spots will appear on the image. These black spots are also called dust artefacts.

The fundus camera consists of a camera, a strobe, an object lens, other lenses, a mirror with a hole, another mirror, some aperture stops and other parts [15], [16]. If dust particles stick to any of these optical components, dust artefacts will be visible on images of the fundus. Previously, two methods of image clarification have been explored: deleting dust artefacts from images and removing house dust from parts of the device. However, these researches did not explore the application of the fundus camera in diagnosing medical

diseases [17]–[21]. Methods of image processing and deleting image artefacts other than dust artefacts have also been used. Moreover, image artefacts were extracted from the existing images [22]–[25]. To our knowledge, no study has reported the effects of flash reflections in airborne dust. We performed some basic experiments to detect dust artefacts for determining whether small retinal haemorrhages due to diabetic retinopathy could be distinguished from dust artefacts using the concept of colour space.

The most important element in the concept of colour space is lightness. House dust is complicated in form and uneven in density. Light volume is irregular due to the diffuse reflection. Dust artefacts create a spotty pattern.

The second most important element is the concentration of colour. In diabetic retinopathy, the fundus is reddish-brown or yellow in colour. Therefore, in this study, red, coffee, ochre and yellow colours were investigated. The CIE and Munsell colour systems can be used to define colours in a colour space [25].

The CIE colour system characterized many colour spaces, including RGB, XYZ and L*a*b*[25]. The RGB colour space has three primary colours: red, green and blue. Because the colour of fundus is closer to red, it is possible to use this colour space, although it is difficult to judge lightness and concentration of colour. As for the XYZ colour space, Y expresses lightness, Z expresses the degree of blueness, and X expresses other elements. Y, corresponding to lightness, can be used for dust artefact detection. Because fundus colour is near red, X may be usable. The "L*" of the L*a*b* colour space expresses lightness and can be used for distinction. Both "a*" and "b*" represent the complementary colours. "a*" represents the colour between red, magenta and green. "b*" represents the colour between yellow and blue. When both "a*" and "b*" are used, they may be able to identify fundus colour. However, there is no means by which the concentration of a colour is distinguishable from other colours.

The Munsell colour system uses the HLS (hue, lightness and saturation) colour space [26]–[28]. Lightness can be used. Since saturation is a numerical value showing the concentration of a colour, it is easy to use. The intermediate colour between red and yellow is orange. Considering that dark orange resembles brown, it is easy to judge the range of red, brown and yellow using a hue circle. Therefore, we adopted the HLS colour space in our study.

To distinguish the small retinal haemorrhages observed in early diabetic retinopathy from dust artefacts, we constructed two experimental devices. One experimental device is a fundamental device that used a magnifier and light bulbs. Using this device, the HLS colour space of dust artefacts was analysed. In a darkroom, one of four different coloured papers was stuck on the ceiling of the experimental device. Using each colour, 10 fragments of house dust particles were photographed using a magnifier. Next, light bulbs of three colours were suspended from the ceiling not stuck with coloured papers, and 10 fragments of house dust particles on the object lens of the camera were again photographed. Finally, the HLS colour space was analysed. In the HLS colour space, lightness distinguished haemorrhages from dust artefacts under all conditions. However, hue and saturation could only distinguish haemorrhages from dust artefacts under certain conditions [29]. The other experimental device was designed to photograph the fundus of artificial eyes. This device has the same optical system as a fundus camera. The HLS colour space of dust artefacts was analysed using this device.

II. METHODS

1.Distinguishing small retinal haemorrhages from dust artefacts using the HLS colour space

Fig.2 (left) shows the division of the fundus image into the haemorrhagic area and the perihaemorrhagic area. Paint Shop Pro v. 8.0 was used to visualize the HLS colour spaces of both these areas, and the RGB values were transformed from the fundus image to the HLS colour space. The hue, lightness and saturation values ranged from 0 to 255. Hue is the actual colour and value is the number assigned on the colour wheel (red = zero, yellow = 43, green = 85, cyan = 128, blue = 170 and magenta = 212). Lightness is the brightness of the hue (zero = black, 128 = middle grey and 255 = white). Saturation is the level of grey added to the hue (zero = very grey and unsaturated and 255 = no grey and fully saturated) [30].

Equation (1) shows the average colour space of the haemorrhagic area **avehm**, and (2) shows the average colour space of the perihaemorrhagic area, **aveph**.

$$\mathbf{avehm} = \begin{bmatrix} AveH\_hm \\ AveL\_hm \\ AveS\_hm \end{bmatrix} \quad (1)$$

$$\mathbf{aveph} = \begin{bmatrix} AveH\_ph \\ AveL\_ph \\ AveS\_ph \end{bmatrix} \quad (2)$$

Fig.2 (right) shows an image of the dust artefact and the periartefact area. Paint Shop Pro v. 8.0 was used to visualize the HLS colour spaces of both these areas.

(3) shows the average colour space of the dust artefact **aveda**, and (4) shows the average colour space of the periartefact area, **avepa**.

$$\mathbf{aveda} = \begin{bmatrix} AveH\_da \\ AveL\_da \\ AveS\_da \end{bmatrix} \quad (3)$$

$$\mathbf{avepa} = \begin{bmatrix} AveH\_pa \\ AveL\_pa \\ AveS\_pa \end{bmatrix} \quad (4)$$

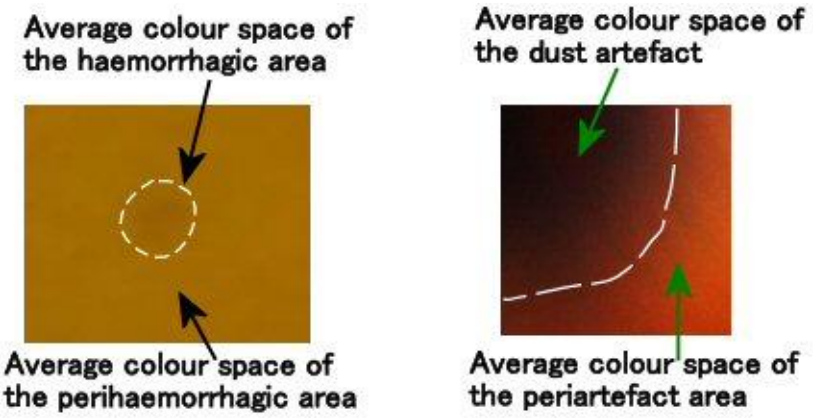

Fig.2 The average colour space of both the haemorrhagic area and the perihaemorrhagic area (left), and the average colour space of the dust artefact and the periartefact area (right)

Hue is generally expressed using 360° of a colour circle [28], [30]–[31]. The average degrees of hue related to a haemorrhage are expressed as **AveHD_hm** and **AveHD_ph**. The average degrees of hue related to a dust artefact are expressed as **AveHD_da** and **AveHD_pa**. (5)–(8) show these average degrees of hue.

$$AveHD\_hm = \frac{AveH\_hm}{255} \cdot 360° \quad (5)$$

$$AveHD\_ph = \frac{AveH\_ph}{255} \cdot 360° \quad (6)$$

$$AveHD\_da = \frac{AveH\_da}{255} \cdot 360° \quad (7)$$

$$AveHD\_pa = \frac{AveH\_pa}{255} \cdot 360° \quad (8)$$

(9)–(12) show the average colour spaces, **AveHm**, **AvePh**, **AveDa** and **AvePa,** using the average degrees of hue.

$$\mathbf{AveHm} = \begin{bmatrix} AveHD\_hm \\ AveL\_hm \\ AveS\_hm \end{bmatrix} \quad (9)$$

$$\mathbf{AvePh} = \begin{bmatrix} AveHD\_ph \\ AveL\_ph \\ AveS\_ph \end{bmatrix} \quad (10)$$

$$\mathbf{AveDa} = \begin{bmatrix} AveHD\_da \\ AveL\_da \\ AveS\_da \end{bmatrix} \quad (11)$$

$$\mathbf{AvePa} = \begin{bmatrix} AveHD\_pa \\ AveL\_pa \\ AveS\_pa \end{bmatrix} \quad (12)$$

DiffH_hm is the difference between the average degrees of hue in the haemorrhagic area and the average degrees of hue in the perihaemorrhagic area. **DiffH_da** is the difference between the average degrees of hue in the dust artefact and the average degrees of hue in the periartefact area. **CngL_hm** is the ratio of change in lightness of the haemorrhagic area to the lightness of the perihaemorrhagic area. **CngS_hm** is the ratio of change in saturation of the haemorrhagic area to saturation of the perihaemorrhagic area. **CngL_da** is the ratio of change in lightness of the dust artefact to the lightness of the periartefact area. **CngS_da** is the ratio of change in saturation of the dust artefact to saturation of the periartefact area. (13) shows the colour space change in the haemorrhagic area **CngHm**, and (14) shows the colour space change in the dust artefact, **CngDa**.

$$\mathbf{CngHm} = \begin{bmatrix} DiffH\_hm \\ CngL\_hm \\ CngS\_hm \end{bmatrix} = \begin{bmatrix} 1 & 0 & 0 \\ 0 & 1/AveL\_ph & 0 \\ 0 & 0 & 1/AveS\_ph \end{bmatrix} \cdot (\mathbf{AveHm} - \mathbf{AvePh}) \quad (13)$$

$$\mathbf{CngDa} = \begin{bmatrix} DiffH\_da \\ CngL\_da \\ CngS\_da \end{bmatrix} = \begin{bmatrix} 1 & 0 & 0 \\ 0 & 1/AveL\_pa & 0 \\ 0 & 0 & 1/AveS\_pa \end{bmatrix} \cdot (\mathbf{AveDa} - \mathbf{AvePa}) \quad (14)$$

(15) shows **AveCngHm**, which is the average of **CngHm**.

$$\mathbf{AveCngHm} = \begin{bmatrix} AveDiffH\_hm \\ AveCngL\_hm \\ AveCngS\_hm \end{bmatrix} \quad (15)$$

(16) shows the colour space for an evaluation, **Ev**, which is the ratio of change of **CngDa** to **AveCngHm**.

$$\mathbf{Ev} = \begin{bmatrix} EvH \\ EvL \\ EvS \end{bmatrix} = \begin{bmatrix} 1/AveDiffH\_hm & 0 & 0 \\ 0 & 1/AveCngL\_hm & 0 \\ 0 & 0 & 1/AveCngS\_hm \end{bmatrix} \times \mathbf{CngDa} \quad (16)$$

2. Fundus photographs of diabetic retinopathy

Fundus photographs were taken in five patients using the fundus camera Topcon TRC-50EX mydriatic retinal camera with a Nikon digital camera D1x. The image sensor was a 23.7 × 15.6-mm, 12-bit RGB CCD [32]. The file format is JPEG baseline-compliant. The number of recorded pixels is 2000 × 1312. Paint Shop Pro v. 8.0 was used to visualize the average colour space of the haemorrhagic area, **avehm,** and the average colour space of the perihaemorrhagic area, **aveph**, in two locations on the photograph.

3. Experimental device

The experimental device, shown in Fig.3, was equipped with an illumination optical system and a photographic optical system separated by a mirror with a hole 4 mm in diameter. The device consists of a canon EOS 50D camera with an EF 50-mm f/1.8-2 camera lens, a Speedlite 270EX flash, an object lens with 50-mm focal length and a centre thickness of 16 mm, four double-convex lenses with focal lengths of 100 mm and centre thicknesses of 10 mm, three aperture stops, a mirror with a hole 4 mm in diameter, another mirror and four artificial eyes. The object lens, four double-convex lenses and two mirrors are all 50 mm in diameter. An MgF2 coating was applied to the surface of all lenses. The image sensor used was a 22.3 × 14.9-mm CMOS sensor [33]. The file format was JPEG, RAW (14-bit Canon original). The number of recorded pixels was 4752 × 3168. Fig. 3 shows the aperture stop equipped with a 13-mm-diameter hole on the right side of the device. The hole in the middle aperture stop was 45 mm in diameter. The aperture stop on the left side of the device was equipped with a 39-mm-diameter hole. Three wires hang a black plate 15 mm in diameter in the centre of the hole.

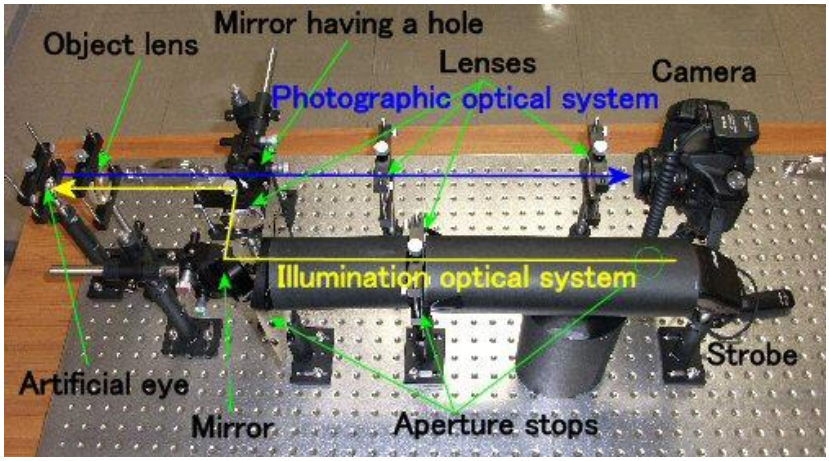

Fig.3 The experimental device

4. Optical system diagram of the experimental device

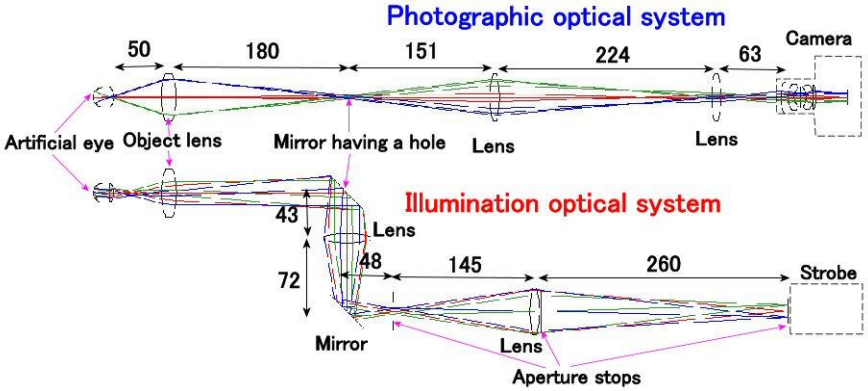

Fig.4 Optical system diagram of the experimental device

The optical system of the experimental device was designed using optical design software (OpTaliX-LT 7.11). Fig.4 shows an illumination optical system and a photographic optical system, including the distance between lenses and the distance between a lens and a mirror per mm. The axial distance from eyeground to the image surface was 797.3 mm and that from eyeground to the strobe surface was 858.9 mm.

5. Artificial eyes

The artificial eye consists of a plane-convex lens, a black spacer with a hole 18 mm in diameter and a hemispherical cup. The plane-convex lens was 20 mm in diameter, with a 4.6-mm centre thickness and a 17.4-mm back focal length. The hemispherical cup was 20 mm in diameter with a thickness of 0.5 mm. The distance from the surface of the plane-convex lens to the eyeground was 22 mm. MgF2 coating was applied to the surface of the plane-convex lens. The hemispherical cup was made of polyethylene terephthalate and painted using four matt colour sprays (Asahipen Corp., Osaka, Japan): red, coffee, ochre and yellow (Fig.5). Ruby red was used as red, Mexican sand was used as coffee, gold amber was used as ochre and canary yellow was used as yellow.

Fig.5 Artificial eye

6. Specimens

We prepared five types of fragments of house dust measuring about 5 × 5 × 5 mm^3. Each fragment was set at points P1–P6 on a lens. Then fragments at each point were photographed one by one, as shown in Fig.6. Paint Shop Pro v. 8.0 was used to visualize the HLS colour space of four areas, as shown in Fig.2.

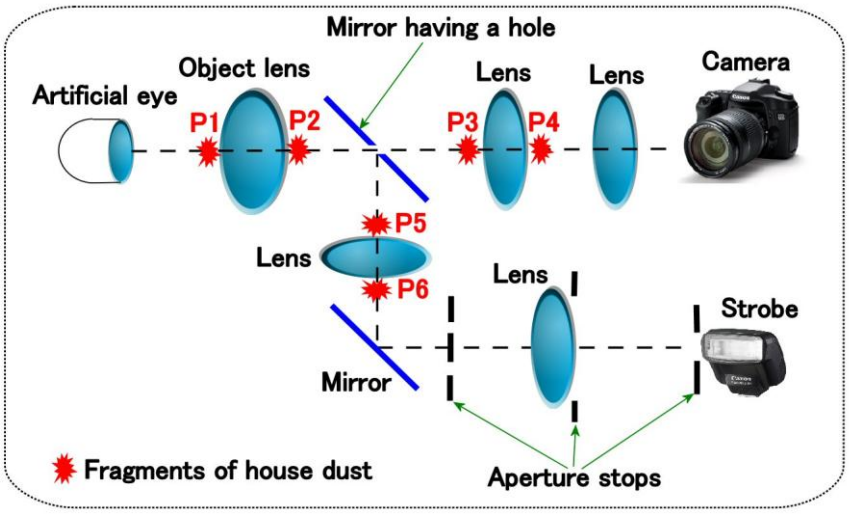

Fig.6 Fragments of house dust were set on the lens at points P1–P6

7. Calculation of evaluation space for house dust using HLS data

(16) shows the colour space for evaluation (**Ev)**, which is the ratio of change of **CngDa** to **AveCngHm**. **CngDa** is the colour space change in the dust artefact and **AveCngHm** is the average of the colour space change in the haemorrhagic area. The greater the absolute values of **EvH**, **EvL** and **EvS**, the greater the extent to which the HLS colour space can be used to distinguish small haemorrhages from dust artefacts. These absolute values must be > 1.0.

III. RESULTS

1.Changed colour spaces of the haemorrhagic area

Fig.7 shows 10 images of small retinal haemorrhagic areas from five fundus images. Paint Shop Pro v. 8.0 was used to visualize both **avehm** and **aveph** in the images. The changed colour space of the haemorrhagic areas is **CngHm**. **CngHm** was calculated by substituting **avehm** and **aveph** in (5), (6), (9), (10) and (13). Table 1 shows the average and standard deviation of **CngHm**.

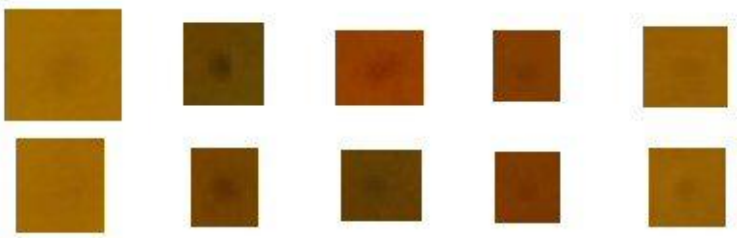

Fig.7 Ten images of the small haemorrhagic area of patients with diabetic retinopathy

Table 1: Changed colour space of haemorrhagic area

Object	Numerical values
DiffH_hm	−1.0°±1.2°
CngL_hm	−0.04±0.02
CngS_hm	−0.01±0.02

2. Evaluation space for house dust on the photographic optical system

Fig.8 shows averages and standard deviations of **EvL** values. Fig.9 shows averages and standard deviations of **EvS** values. The averages are shown as bar graphs and the standard deviations are shown as lines. Table 2 shows averages and standard deviations of the **EvH** value. These values are obtained from the photographs of fragments of house dust at points P1, P2, P3 and P4. According to Fig.8, the average **EvL** values

were as follows: ochre 4.2–10.2, coffee 5.1–12.4, red 7.0–12.0 and yellow 7.3–15.1. The average **CngL_da** values of all colours were 4.1 times higher than the **AveCngL_hm** values. This shows that "|**CngL_da**| > |**AveCngL_hm**|" was consistently dominant.

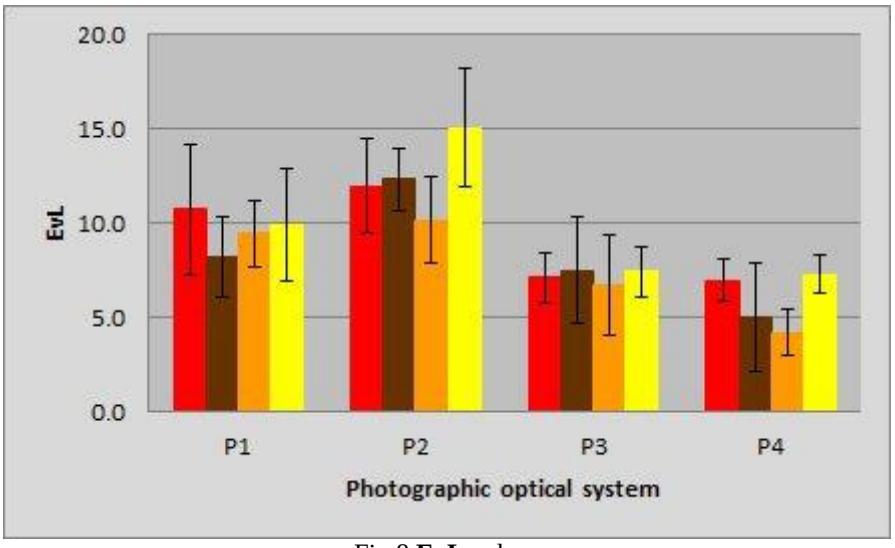

Fig.8 **EvL** values

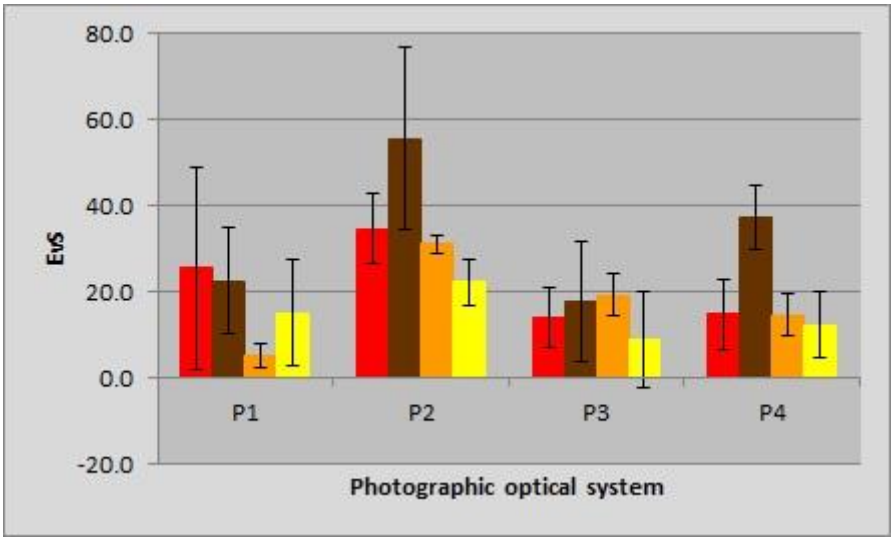

Fig.9 **EvS** values

Table 2: EvH values

Colour	P1	P2	P3	P4
Red	−7.1±16.9	−37.7±32.2	0.3±1.2	0.3±1.2
Coffee	−5.7±7.4	−5.1±3.0	−0.6±1.6	−2.0±1.9
Ochre	0.3±2.3	−1.7±2.3	−2.6±2.3	−1.7±1.2
Yellow	3.4±1.6	0.0±5.8	1.1±3.1	0.6±3.9

Lightness can be used to distinguish small haemorrhages from dust artefacts. According to Fig.9, the average **EvS** values were as follows: ochre 5.0–31.1, yellow 9.0–22.3, red 14.0–34.7 and coffee 17.8–55.6. Standard deviations of **EvS** values for the combination of yellow and P3 were high. This shows that "|**CngH_da**| > |**AveCngH_hm**|" was consistently dominant, except for the combination of yellow and P3. Saturation can be used to distinguish small haemorrhages from dust artefacts, except for the combination of yellow and P3. According to Table 2, the absolute values of the average **EvH** were >1.7 in the following combinations: coffee and P2, ochre and P4 and yellow and P1. In these combinations, the standard deviations of **EvH** values were low; thus, hue can be used to distinguish small haemorrhages from dust artefacts in these cases.

3. Evaluation space for house dust on the illumination optical system

Fig.10 shows averages and standard deviations of **EvL** values. Fig.11 shows averages and standard deviations of **EvS** values. The averages are shown as bar graphs and the standard deviations are shown as lines. Table 3 shows the average and standard deviation of the **EvH** value. These values are obtained from the photographs of fragments of house dust at points P1, P2, P5 and P6. According to Fig.10, the average **EvL** values were as follows: ochre 3.1–10.2, coffee 4.2–12.4, red 4.9–12.0 and yellow 6.0–15.1. The average **CngL_da** values of all colours were 3.1 times higher than the **AveCngL_hm** values. This shows that "|**CngL_da**| > |**AveCngL_hm**|" was consistently dominant.

As with the photographic optical system, lightness can be used to distinguish small haemorrhages from dust artefacts. According to Fig.11, the average **EvS** values were as follows: coffee −2.5–55.6, red 2.7–34.7, ochre 5.0–31.1 and yellow 13.3–22.3. Standard deviations of **EvS** values were high for the following combinations: coffee and P5, red and P5 and ochre and P5. This shows that "|**CngH_da**| > |**AveCngH_hm**|" was consistently dominant except for these combinations. Saturation can be used to distinguish small haemorrhages from dust artefacts except for these combinations. According to Table 3, the absolute values of the average **EvH** were >1.7 in the following combinations: red and P5, red and P6, coffee and P2, coffee and P6, ochre and P6, yellow and P1, yellow and P5 and yellow and P6. In these combinations, standard deviations of **EvH** values were low; thus, hue can be used to distinguish small haemorrhages from dust artefacts in these combinations.

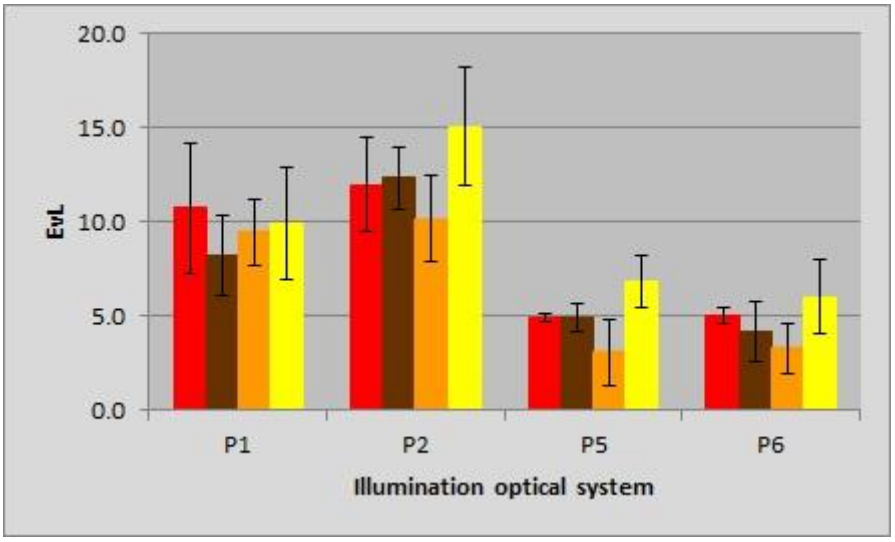

Fig.10 **EvL** values

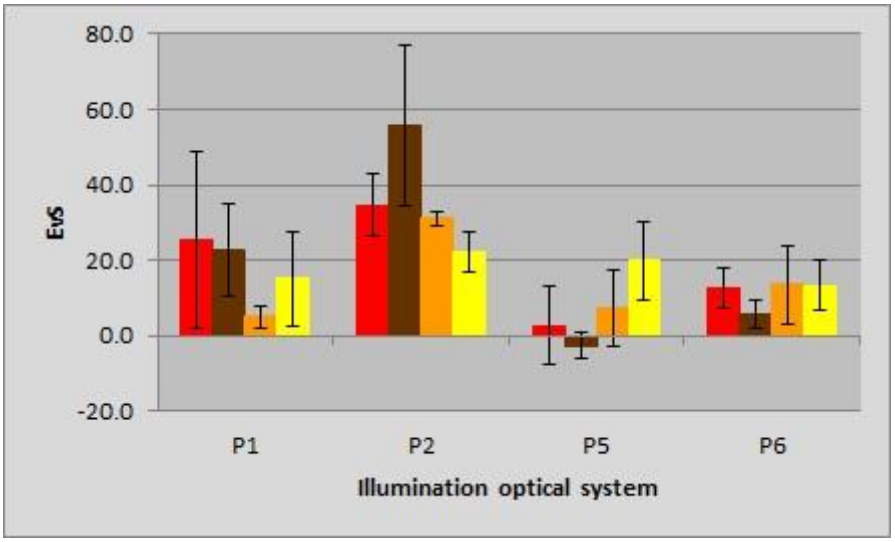

Fig.11 **EvS** values

Table 3: EvH values

Colour	P1	P2	P5	P6
Red	−7.1±16.9	−37.7±32.2	2.6±0.6	2.0±0.8
Coffee	−5.7±7.4	−5.1±3.0	0.9±1.3	1.7±1.2
Ochre	0.3±2.3	−1.7±2.3	−1.1±0.6	−2.3±1.3
Yellow	3.4±1.6	0.0±5.8	−2.6±1.6	−2.9±1.0

IV. CONCLUSION

We constructed an experimental device with the same optical system as a fundus camera, but with the addition of four different coloured artificial eyes. We investigated various methods of distinguishing small retinal haemorrhages caused by diabetic retinopathy from dust artefacts using the HLS colour system. In the HLS colour space, lightness and saturation enabled distinction of haemorrhages from dust artefacts under almost all conditions; however, hue enabled this distinction under certain conditions only. Lightness was particularly highly sensitive. Saturation was also highly sensitive in most conditions. Therefore, it is possible to distinguish small retinal haemorrhages from dust artefacts automatically using our device if lightness and saturation are used. Fragments of house dust of $5 \times 5 \times 5$ mm^3 were used as specimens. Future studies are required to investigate the minimum detectable size of house dust. In addition, we will attempt to distinguish not only small retinal haemorrhages but also hard exudates, such as microaneurysms, using this device.

V. Acknowledgements

Photographs from diabetic retinopathy patients were provided by Hiroshima University Hospital. For research expenses, the intramural budget of Hiroshima International University was used. We are very thankful to all those who helped in our research.

REFERENCES

[1] Z.T. Bloomgarden, American Diabetes Association Annual Meeting, 1999, Diabetes and obesity, *Diabetes Care 23(1)*, 2000, 118-124
[2] T. Tsuchiya, Measure Against Lifestyle Related Disease, *JMAJ 49(3)*, 2006, 132-134
[3] S. S. Savant and H. B. Chandalia, Diabetic retinopathy, *Intnl. J. Dev. Contries 10*, 1991, 9-25
[4] American Diabetes Association, Diabetic retinopathy, *Clinical Diabetes19(1)*, 2001, 29-32
[5] J. B. Brown, K. L. Pedula, K. H. Summers, Diabetic retinopathy, *Diabetes Care 26(9)*, 2003, 2637-2642.
[6] E. Duh, Diabetic Retinopathy, Humana Press, 2008, 29-66
[7] S. Garg and R. M. Davis, Diabetic retinopathy screening update, *Clinical diabetes 27(4)*, 2009, 140-145.
[8] I. U. Scott, N. M. Bressler, S. B. Bresseler et al, Agreement between clinical and reading center gradings of diabetic retinopathy severity level at baseline in a phase 2 study of intravitreal bevacizumab for diabetic macular edema, *Retina 28(1)*, 2008, 36-40.
[9] M. S. Figueroa, I . Contreras, S. Noval, Anti-angiogetic drugs as an adjunctive therapy in the surgical treatment of diabetic retinopathy, *Curr Diabetes Rev. 5(1)*, 2009, 52-56.
[10] E. Fernández-Caldas, W. L. Trudeau and D. K. Ledford, Environmental control of indoor biologic agents. *J. Allergy. Clin. Immunol. 2(2)*, 1994, 404-412.
[11] A.G. Oomen, J. P. C. M. Janssen, A. Dusseldorp et al., Ecposure to chemicals via house dust, *RIVM Report 609021064/2008*, 2008, 11-18.
[12] M. Born and E. Wolf, Principles of Optics 7th expanded edition, Electromagnetic Theory of Propagation, Interference and Diffraction of Light, Cambridge Univ. Press, 1999, 142-227.
[13] R. G. Willson, M. W. Maimone, A. E. Johnson et al, An Optical Model for Image Artifacts Produced by Dust Particles on Lenses, *Proc. ISAIRAS 2005 Conference*, 2005, ESA SP 603.
[14] A.V. Shukla, Clinical Optics Primer for Ophthalmic Medical Personnel, A Guide to Laws, Formulae, Calculations, and Clinical Applications, SLACK Inc. 2009, 85-89.
[15] D. D. David, R. Prescott, and S. Kennedy, Simultaneous stereoscopic fundus camera incorporating a single optical axis, *Invest. Ophthalmol. Vis. Sci. March*, 1980, 289-297.
[16] R. Zeimer, S. Zou, T. Meeder et al, A fundus camera dedicated to the screening of diabetic retinopathy in the primary-care physician's office, *IOVS May 43(5)*, 2002, 1581-1587
[17] R. F. Lyon, Prism-Based Color Separation for Professional Digital Photography, *Proceedings of IS&T's PICS 2000 Conference: Image Processing, Image Quality, Image Capture Systems Conference*, Oregon, 2000, 50-54.
[18] A. E. Dirik, H. T. Sencar and N. Memon, Source Camera Identification Based on Sensor dust Characteristics, *Signal Processing Applications for Public Security and Forensics 2007, SAFE'07, IEEE Workshop*, 2007, 1-6.
[19] A. Zamfir, A. Drimbarean, M. Zamfir et al., An Optic Model of the Appearance of Blemishes in Digital Photographs, *Proceedings of SPIE, Vol. 6502, Digital Photography 3*, 2007.
[20] R. Bergman, R. Maurer, H. Nachlieli et al, Comprehensive Solutions for Removal of Dust and Scratches from Images, *Journal of Electronic Imaging 17(1)*, 2008, 1-25.
[21] A. E. Dirik, H. T. Sencar and N. Memon, Digital Single Lens Reflex Camera Identification From Traces of Sensor Dust, *IEEE Trans. Info. For. and Sec.3(3)*, 2008, 539-552.
[22] P. J. Saine, Errors in Fundus Photography, *Journal of Ophthalmic Photography 7(2)*, 1984, 120-122.
[23] H. Narasimha-Iyer, A. Can, B. Roysam et al., Robust Detection and Classification of Longitudinal Changes in Color Retinal Fundus Images for Monitoring Diabetic Retinopathy, *IEEE Trans. Biomed. Eng. 53(6)*, 2006, 1084-1098.
[24] H. Narasima-lyer, A. Can, B. Roysam et al, Integrated analysis of vascular and nonvascular changes from color retinal fundus image sequences., *IEEE Trans Biomed Eng. 54(8)*, 2007, 1436-1445
[25] J. Koenderink, Colour for the sciences, The MIT Press, 2009, 45-52, 497-537.

[26] B. Jahne, Practical Handbook on Image Processing for Scientific Applications, CRC Press, 1997, 102-107.
[27] B. G. Haskell, A. Puri and A. N. Netravali, Digital Video: An Introduction to MPEG-2, Chapman & Hall, 1997, 86-91.
[28] A. Hanbury and J. Serra, Mathematical Morphology in the HLS Colour Space, *12th British Machine Vision Conference, Manchester, UK*, 2001, 451–460.
[29] N. Suzuki, Basic Research for Distinguishing Small Retinal Hemorrhages from Dust Artifact by using Hue, Lightness, and Saturation Color Space, *World Academy of Science, Engineering and Technology 65*, 2012, 844-852.
[30] Jasc Software, Inc., Chapter 8: Making color and Tonal Corrections, Paint Shop Pro 8 User Guide, 2002, 181-206.
[31] R. A. Peters II, Mathematical morphology for angle-valued images, *Proceedings of the SPIE, Nonlinear Image Processing VIII 3026*, 1997, 84-94.
[32] Nikon Corporations, Nikon D1X Operators Manual, 212-219
[33] Canon Inc., Canon EOS 50D Instruction Manual,2008, 204-210